Fernández Sáez, J.; Bonastre Cano, JA.; Molina Puerto, J.; Del Río García, AI.; Cases Iborra, FJ. (2017). Study on the specific capacitance of an activated carbon cloth modified with reduced graphene oxide and polyaniline by cyclic voltammetry. European Polymer Journal. 92:194-203. doi:10.1016/j.eurpolymj.2017.04.044.

Manuscript Details

Manuscript number	EUROPOL_2017_70
Title	Study on the specific capacitance of an activated carbon cloth modified with reduced graphene oxide and polyaniline by cyclic voltammetry
Article type	Research paper

Abstract

This work describes a two-step process for the electrochemical coating of reduced graphene oxide (RGO) and polyaniline (PANI) onto an activated carbon cloth (ACC) by cyclic voltammetry (CV). The fact that the two syntheses are carried out independently of each other, makes it possible to select the experimental conditions for each one and to study the electrochemical response of RGO, PANI, and PANI onto RGO (RGOPANI), separately. Thus, by modifying the potential limits of the aniline-polymerization reaction, it was possible to observe the influence of RGO and the maximum amount of PANI that the carbon cloth can receive in terms of proper electrochemical response. Electrochemical properties were characterized by CV, galvanostatic charge-discharge curves (using three or two-electrodes symmetric cell configurations) and electrochemical impedance spectroscopy (EIS). A maximum improvement of 25%, 56% and 61% over the initial specific capacitance of ACC (about 129 F g-1) were obtained for RGO, PANI and RGOPANI coatings, respectively. Good cycling stability retaining 83% of the initial capacitance, after 1000 cycles stability test, was obtained for RGOPANI sample. Promising results of energy and power densities were also achieved. In the analyses by Fourier transform infrared spectroscopy (FTIR), the PANI-bands could be clearly identified which is indicative of a significant presence of PANI. Field emission scanning electron microscopy (FESEM) showed the morphology of RGO, PANI and RGOPANI onto the ACC fibers. These analyses helped to explain the electrochemical results.

Keywords	Activated carbon cloth; reduced graphene oxide; polyaniline; aniline adsorption; capacitance.
Manuscript category	Regular Paper

Corresponding Author	Francisco Cases
Order of Authors	Javier Fernández, José Bonastre, Javier Molina, Ana del Río, Francisco Cases

Suggested reviewers	Juan Carlos Galvan, Hui-Ming Cheng, Ryszard Fryczkowski, Ryuji Hirase, Mahdi Nouri

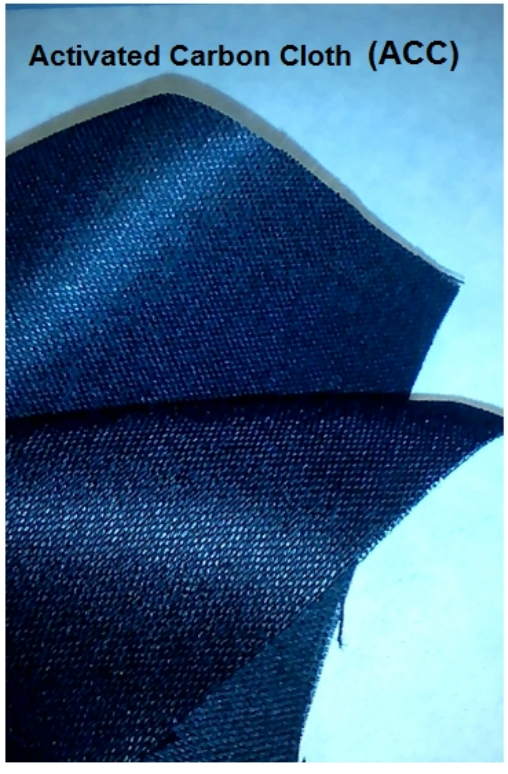
Activated Carbon Cloth (ACC)

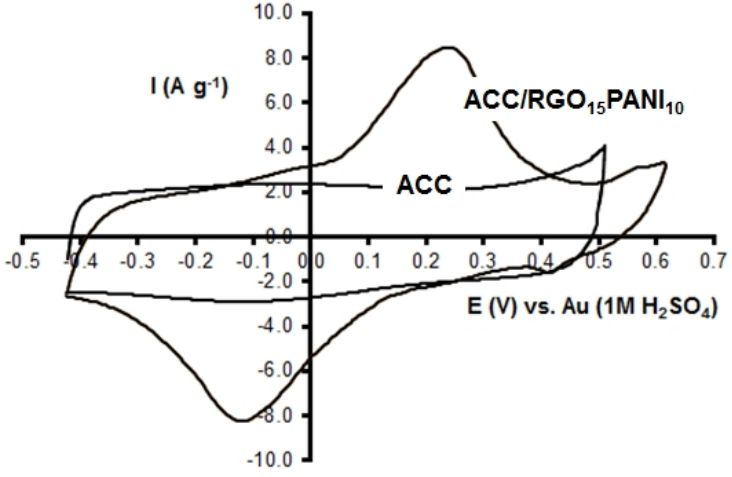
I (A g-1)
ACC/RGO15PANI10
ACC
E (V) vs. Au (1M H2SO4)

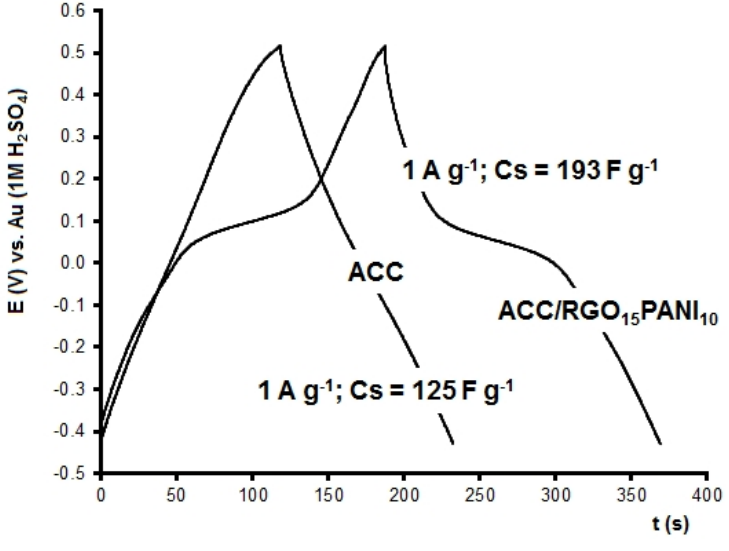
E (V) vs. Au (1M H2SO4)
1 A g-1; Cs = 193 F g-1
ACC
ACC/RGO15PANI10
1 A g-1; Cs = 125 F g-1
t (s)

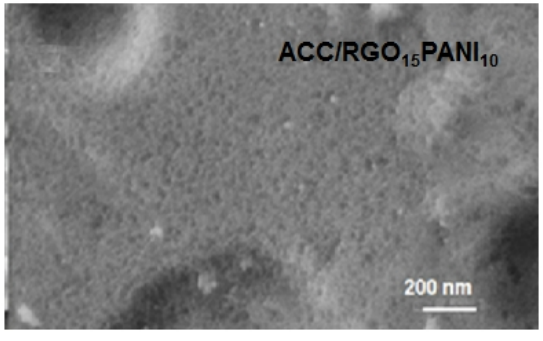
ACC/RGO15PANI10
200 nm

Study on the specific capacitance of an activated carbon cloth modified with reduced graphene oxide and polyaniline by cyclic voltammetry

J. Fernández [a], J. Bonastre [a], J. Molina [a], A. I. del Río [a], F. Cases [a, *]

[a] *Departamento de Ingeniería Textil y Papelera, Escuela Politécnica Superior de Alcoy, Universitat Politècnica de València, Plaza Ferrándiz y Carbonell, s/n, 03801 Alcoy,* Spain

Abstract

This work describes a two-step process for the electrochemical coating of reduced graphene oxide (RGO) and polyaniline (PANI) onto an activated carbon cloth (ACC) by cyclic voltammetry (CV). The fact that the two syntheses are carried out independently of each other, makes it possible to select the experimental conditions for each one and to study the electrochemical response of RGO, PANI, and PANI onto RGO (RGOPANI), separately. Thus, by modifying the potential limits of the aniline-polymerization reaction, it was possible to observe the influence of RGO and the maximum amount of PANI that the carbon cloth can receive in terms of proper electrochemical response. Electrochemical properties were characterized by CV, galvanostatic charge-discharge curves (using three or two-electrodes symmetric cell configurations) and electrochemical impedance spectroscopy (EIS). A maximum improvement of 25%, 56% and 61% over the initial specific capacitance of ACC (about 129 F g^{-1}) were obtained for RGO, PANI and RGOPANI coatings, respectively. Good cycling stability retaining 83% of the initial capacitance, after 1000 cycles stability test, was obtained for RGOPANI sample. Promising results of energy and power densities were also achieved. In the analyses by

Fourier transform infrared spectroscopy (FTIR), the PANI-bands could be clearly identified which is indicative of a significant presence of PANI. Field emission scanning electron microscopy (FESEM) showed the morphology of RGO, PANI and RGOPANI onto the ACC fibers. These analyses helped to explain the electrochemical results.

Keywords: Activated carbon cloth; reduced graphene oxide; polyaniline; aniline adsorption; capacitance.

* Corresponding author. Tel.: +34 96 652 84 12; fax: +34 96 652 84 38.

E-mail address: fjcases@txp.upv.es (F. Cases).

1. Introduction

Activated carbons are of special interest due to the exceptional physical and chemical properties that they possess, such as porosity, high surface area, adsorption capacity, chemical stability, corrosion resistance, thermal resistance and electrical conductivity [1-4]. Activated woven carbon cloths are very promising materials because they provide continuous current paths that reduce the interparticle resistance [5]. In addition, the mechanical properties of textile materials, such as weigh and flexibility, add new possibilities to the design of energy storage devices [6]. Supercapacitators have attracted considerable attention in recent years because of their high power density, long life cycle, and potential applications [5]. However, the capacitance of carbon materials is low, and this is the reason why carbon materials are coated with pseudo-capacitive materials such as conductive polymers. Polyaniline (PANI) is good candidate for energy storage devices due to its ease of synthesis, environmental stability, fast redox activity and high specific capacitance [5-23]. Graphene has attracted much attention during recent years due to its

unique electronic and mechanical properties [24], high specific surface area, high electron mobility at room temperature and ability to sustain high electric currents densities [25, 26]. Reduced graphene oxide (RGO) not only has good electrical properties and a large conjugated aromatic ring which can interact with porous carbon materials, but also many functional groups that can chemically interact with conducting polymers [5]. For the synthesis of RGO from graphene oxide (GO), several reducing agents such as *p*-phenylene diamine [5], glucose [11], aniline [14], hydrazine [9, 17, 18] and L-cysteine [16] have been tried. For the synthesis of PANI, persulfate salts were used to oxidize aniline [9, 14, 17, 18]. The use of reducing agents for the GO reduction and oxidizing agents for the aniline oxidation makes these processes more expensive, arduous, and less environmentally friendly. Thus, electrochemical synthesis is seen as a good alternative to the use of chemicals. Different materials such as copper foil [10], glassy carbon [10, 13, 20], foamed nickel [10], Pt-plate [10] and indium tin oxide [20] were used as base of the graphene-PANI electroactive material for working electrodes. From a more practical point of view, the graphene-PANI material was anchored to different substrates. The flexibility of the substrate for electrodes has captured the attention of a number of researchers. Thus, flexible materials such as activated carbon cloth [5, 16] or paper [6] have been cited as substrate for working electrodes. Flexible 3D-structures of graphene/polyaniline have also been reported [15, 16, 23] for supercapacitors.

On the basis of the above, the present work aims to modify the capacitance of an activated carbon cloth (ACC) by electrochemical coating of RGO and PANI on its surface. Both direct electrosyntheses were carried out by CV using a small piece of ACC as working electrode (WE). CV, EIS, and galvanostatic techniques were used for the electrochemical characterization of the different samples. A test-cell (Swagelok-type cell) dedicated to the characterization of aqueous battery and capacitor systems, wired up for three or two

electrode testing, was used for this purpose. The surface morphologies and chemical structures were characterized by FESEM and FTIR, respectively. To assess the deliverable performance for real-life applications, the energy and power densities were calculated from the charge-discharge curves for the two-electrode symmetric cell.

2. Experimental

2.1. Reagents and chemicals

Monolayer graphene oxide (GO) powders were acquired from Nanoinnova Technologies S.L. (Spain). Lithium perchlorate ($LiClO_4 \cdot 3H_2O$), analytical grade sulphuric acid (H_2SO_4) and aniline were purchased from Merck. Aniline was purified by distillation before use. Distillation was performed at reduced pressure in order to avoid thermal degradation of the monomer. After distillation, aniline was stored in the dark at 5 ºC. Ultrapure water was obtained from an Elix 3 Millipore-Milli-Q Advantage A10 system with a resistivity near to 18.2 mΩ cm. The solutions for the CV-syntheses were deoxygenated by bubbling nitrogen gas (N_2 premier X50S).

2.2. Electrodes

The surface (3 mm diameter disc) of a glassy carbon electrode (GCE) was polished with 0.05 μm alumina and then thoroughly rinsed with water. The voltammetric study, using the GCE as working electrode, was carried out in a conventional voltammetric cell of three electrodes. A 3 g L^{-1} GO and 0.1 M $LiClO_4 \cdot 3H_2O$ solution was used for the RGO synthesis. The characterization of GCE/RGO was performed in a 0.1 M $LiClO_4 \cdot 3H_2O$ solution.

The company Chemviron Carbon supplied the activated carbon woven cloth Zorflex® FM10, 0.5 mm thick with a surface density of 120 g m^{-2}. The textile electrodes (WEs)

were prepared by cutting a 1 cm x 3 cm strip from the carbon fabric. A proper electric contact was obtained by gluing the textile samples to 2 mm diameter copper rods, with the tip flattened to improve the electric contact, using CircuitWorks® conductive epoxy resin by Chemtronics®. The resin was hardened in an oven at 90 ºC and the joint was wrapped with Teflon tape and glued with epoxy resin to isolate it from the solution. WEs will be used as working electrodes for the RGO and PANI syntheses.

2.3. Electrochemical cells

The CV-coating onto WEs were carried out in a conventional cell for voltammetry equipped with a Pt cylindrical mesh (6 cm height and 3 cm diameter) for the RGO synthesis or a stainless steel cylindrical mesh (4 cm height and 3 cm diameter) for the aniline polymerization, as counter electrodes (CE). The reference electrode was an Ag/AgCl (3 M KCl). The WE was placed in the center of the cylinder and 3 cm^2 (geometrical area) was introduced into the solution. The solution 3 g L^{-1} GO and 0.1 M $LiClO_4 \cdot 3H_2O$ was sonicated with the aid of an ultrasound bath for 30 min for the dispersion of GO monolayer powders. During the CV-experiments, the GO-solution was gently stirred to avoid the precipitation of GO. The 0.2 M aniline solution was prepared by dissolving freshly distilled aniline in 1.0 M H_2SO_4 solution. The electrochemical characterization of the textile samples was carried out in a test-cell (Swagelok-type cell) ECC-Aqu from EL-CELL. The parts of the cell that come in contact with the electrolyte are made of fine gold and thermoplastic polymer PEEK. Two textile samples of 0.5 cm x 0.5 cm (cut from WE) were positioned in parallel on both sides of the separator and at the same time, between the two circular gold current collector (2 cm diameter). These samples were described as ACC/RGO_aPANI_b, where subscripts “a” and “b” are the number of cycles of synthesis.

The separator is a circular piece (2 cm diameter) of glass fiber filter, 0.3 cm thick, 1.2 μm nominal pore size, soaked with 1 M H_2SO_4 solution. The test-cell worked in three-electrode or two-electrode symmetric configurations. In the three-electrode configuration, a gold metal pin was the reference electrode (RE). The reference electrode potential was -0.3 V vs. Ag/AgCl under the experimental conditions. RE was positioned close to the separator edge in between the working and the counter electrode (current collectors). In the two-electrode configuration, the RE-cable of the Autolab PGSTAT was connected to that for the CE. The electrochemical performance was analyzed by galvanostatic charge-discharge curves. The specific capacitance (Cs, F g^{-1}) was calculated by Eq (1): $Cs = It/Vm$ where I is the discharged current (A), t is the discharge time (s), V is the potential change during discharge process (V), and m is the mass of one piece of the active material including the activated carbon cloth (g). In the voltammetric studies, the current is expressed in terms of density current (A g^{-1}).

All the electrochemical studies of the present paper were carried out with an Autolab PGSTAT302 potentiostat/galvanostat. The ohmic potential drop was measured and introduced in the Autolab software (GPES).

2.4. Surface morphology and chemical structure characterization

A Zeiss Ultra 55 field emission scanning electron microscope (FESEM) was used to observe the morphology of the samples using an acceleration voltage of 3 kV. The FTIR spectra were recorded with a spectrophotometer FTIR NICOLET 6700 equipped with a horizontal-ATR accessory. The material of the ATR prism is cinc selenide. The spectra were recorded at 400 scans and with a resolution of 4 cm^{-1}.

3. Results and discussion

3.1. Electrochemical syntheses of RGO and PANI

Both RGO synthesis and aniline polymerization were carried out by CV. The choice of potentiodynamic method was due to the internal resistance of the WE. Although the ohmic drop is measured and introduced in the software of the Autolab, a potentiostatic synthesis provoked a fast drop of the current making the coating of a significant amount of RGO or PANI onto the WE surface impossible. In addition, Choi [27] demonstrated that potentiodynamically synthetized PANI shows better adherence, and optical and morphological characteristics than the potentiostatically synthetized PANI. Different potential limits and scan rates were selected for the aniline polymerization. Thus, a WE was cycled from -0.12 V to 1.10 V in the 0.2 M aniline solution at scan rates of 20 mV s^{-1} and 5 mV s^{-1}. The CV-curves recorded during the PANI synthesis at a scan rate of 5 mV s^{-1} are shown in Fig. 1. Only at a scan rate of 5 mV s^{-1} it is possible to observed the current change between 0.82 V and 1.10 V which is evidence of the polymerization process. Nevertheless, a CV-synthesis carried out between -0.12 V and 0.82 V, at a scan rate of 20 mV s^{-1} for 50 cycles, provided valuable results as discussed later in this paper. The experiments with 20 and 15 cycles, in the -0.12 V to 1.10 V range, at a scan rate of 5 mV s^{-1}, resulted in a massive polymerization of PANI by forming a thick layer on the textile surface that came easily off when rinsed with the sulphuric solution 1.0 M. Moreover, a poor electrochemical response was obtained when these samples were analyzed in the test-cell. Because of that, ten cycles, are considered to be the limit to the amount of PANI that is electrochemically effective.

To study the influence of RGO on the aniline polymerization, the surface of WE was previously coated by CV in the GO/$LiClO_4$ solution. No characteristic peaks were observed in the CV-curves even at low scan rates (10 mV s^{-1} and 5 mV s^{-1}). For that

reason, the selection of the potential range was based on a previous study (not included) using GC and Pt wire electrodes. Figs. 2a and b show the CV-curve of the second cycle for the GCE/RGO synthesis at the reduction potential limits of -1.80 V and -1.60 V for 20 cycles at a scan rate of 50 mV s^{-1}. A large cathodic current wave at -1.45 V with an onset at -0.95 V is observed. This wave is attributed to the reduction of the oxygen containing groups (hydroxyl and epoxy groups) on GO [28]. Accordingly, a potential range of -1.60 V to 0.60 V was chosen for the reduction of GO on WE. The effect of the 15 cycles for the RGO synthesis was tested in both voltammetric and galvanostatic studies.

3.2. Electrochemical and spectroscopic characterization of ACC and ACC/RGO

Fig. 3a shows the CV-curve obtained for ACC at a potential range from -0.42 V to 0.52 V at a scan rate of 20 mV s^{-1}. One pair of inconspicuous redox peaks, attributed to the transition between quinone/hydroquinone states [11], can be seen. Its rectangular shape is characteristic of the electric double-layer capacitance of carbon-based materials. In Fig. 3b, the charge-discharge curves for the fifth cycle, at different current densities of 1, 2, 3 and 4 A g^{-1}, are shown. The specific capacitance was estimated in 125 F g^{-1} at the current density of 1 A g^{-1}. In Fig. 3c the enlarged voltammetric area for ACC/RGO_{15} can be seen, which is indicative of its enhance storage capacity. A 30% increase in the specific capacitance was estimated from the charge-discharge curves of Fig. 3d. In Fig.3e, a FESEM-micrograph of ACC/RGO_{15} is shown. RGO structures appeared as well-packed graphene layered structures with films that are at times folded or continuous. It is possible to distinguish the edges of individual sheets, including kinked and wrinkled areas.

3.3. Electrochemical and spectroscopic characterization of ACC/PANI and ACC/RGOPANI samples

Figs. 4 and b show the CV-curves of first and stabilized cycles for ACC/$PANI_{50}$ and ACC/$RGO_{15}PANI_{50}$. The stabilized CV-curves show a couple of peaks, at about 0.14 V, asserted to the reversible leucoemeraldine/emeraldine transition. This peak is absent in the first cycle of ACC/$PANI_{50}$ and very early for ACC/$RGO_{15}PANI_{50}$, indicating that the polymerization of aniline at 0.82 V did not happen, in this case, in a meaningful way. The voltammetric peak at 0.40 V was attributed to the oxidation of the adsorbed aniline. This peak disappeared with the progress of the polymerization. The current peaks of the leucoemeraldine/emeraldine transition reached values of 4.7 A g^{-1} and 7.5 A g^{-1} for ACC/$PANI_{50}$ and ACC/$RGO_{15}PANI_{50}$, respectively. Taking into account that the current peaks corresponding to the aniline oxidation reached similar values, it is considered that the increment of the current peak for ACC/$RGO_{15}PANI_{50}$ is due to the contribution of RGO to the formation of a more highly conductive and electrochemically active PANI. The Figs. 4c-d and 4e-f show the FESEM-images of ACC/$PANI_{50}$ and ACC/$RGO_{15}PANI_{50}$, respectively. The carbon surface of ACC/$PANI_{50}$ appears clean, without the presence of PANI. This result agrees with that observed in the first cycle of CV-curves in Fig. 4a. Fig. 4e shows the RGO structure as a veil that covers the carbon fibers of the cloth. Certain globular structures of PANI can be distinguished in the image of Fig. 4f. These structures could be responsible of the small lump observed in the first scan of the CV-curve depicted in Fig. 4b.

Figs. 5a and b show the CV-curves of ACC/$PANI_{10}$ and ACC/$RGO_{15}PANI_{10}$. In this case, the first cycle of both samples shows the peak associated with the leucoemeraldine/emeraldine transition. This result indicates that the potential limit 1.10 V is high enough to provoke the polymerization of aniline on the surface of ACC. In

addition, the current peaks of the leucoemeraldine/emeraldine transition in the stabilized CVs reached similar density current values (8.5 A g^{-1} for ACC/$RGO_{15}PANI_{10}$ and 8.9 A g^{-1} for ACC/$PANI_{10}$). Nevertheless, a broader peak is obtained for RGO sample which suggests a higher capacitive behavior. By comparison, when the polymerization of aniline occurs in a meaningful way at the potential limit of 1.10 V, the contribution of RGO is less than in the previous case for ACC/$PANI_{50}$ and ACC/$RGO_{15}PANI_{50}$. The Figs. 5c-d and 5e-f show the FESEM-images of ACC/$PANI_{10}$ and ACC/$RGO_{15}PANI_{10,}$ respectively. In this case, both images show a clear layer of PANI coating the carbon fibers. Moreover, the structure of PANI with RGO is more compact, smoother and with less pores than PANI on bare carbon fiber.

Similar FTIR-spectra were obtained for ACC/$PANI_{10}$ and ACC/$RGO_{15}PANI_{10}$. In accordance with scientific literature [29-40], some characteristic bands could be associated with the presence of PANI. The spectrum for the carbon cloth is included as reference. Thus, in the FTIR-spectra of Fig. 6 the following were identified:

- The bands between 1610 cm^{-1} and 1640 cm^{-1} are attributed to C=N bonds stretching vibration [30].
- The 1575 cm^{-1} band is identified with C=C bonds stretching vibration in the quinoid rings [30, 33-35].
- The band centred at 1506 cm^{-1} is related to C=C bonds stretching vibration in the benzenoid rings [30, 33-35].
- The band centred at 1300 cm^{-1} is attributed to C-N bonds stretching vibration of the secondary amines probably related to the leucoemeraldine component [30, 38].
- The band at 1200 cm^{-1} is identified with C-N bonds stretching vibration [37].

- The band at 1130 cm^{-1} is attributed to C-C stretching vibration in the quinoid rings [32] although it is likely that the sulfate anion present in PANI structure contributes to this [30].
- The bands at 1025 cm^{-1} and 860 cm^{-1} could be attributed to C–H in plane bending of 1, 4-ring [36] and C–H out-of-plane bending of 1, 2, 4 ring [30, 32, 33, 39].
- The band centred at 795 cm^{-1} is related to N–H out-of-plane bending [40] and the bands between 710-750 cm^{-1} is associated to C–H out-of-plane bending of 1, 2-ring [39] or C-C out of plane bending vibration [30].
- The band centred at 1695 cm^{-1} could have a major contribution of carboxylic species of the carbon substrate as consequence of the porous structure of PANI.

Figs. 7a-d show the charge-discharge plots of ACC/$PANI_{50}$, ACC/$RGO_{15}PANI_{50}$, ACC/$PANI_{10}$ and ACC/$RGO_{15}PANI_{10}$. Two voltage stages are observed. The first stage (from about 0.4 V to -0.1 V) is due to the combination of pure electric double layer and faradaic capacitances, and the second stage (from -0.1 V to -0.4 V) is associated to pure electric double layer capacitance, whose discharging duration is shorter. The specific capacitance for ACC was estimated in 125 F g^{-1} at a current density of 1 A g^{-1}. Thus, a 54% increase of the specific capacitance was obtained for ACC/$RGO_{15}PANI_{10}$. The charge-discharge curves at current densities of 2, 3 and 4 A g^{-1} demonstrated that the specific capacitance is mainly based on the current density. In addition, the specific capacitance is decreased with the increase of the current density. The decrease of the specific capacitance with the current density for ACC/$PANI_{50}$ and ACC/$RGO_{15}PANI_{50}$ is about 8% while for ACC/$PANI_{10}$ and ACC/$RGO_{15}PANI_{10}$ it is between 15% and 13%. This feature suggests that both $PANI_{50}$ samples exhibit better rate capability

characteristics at high current densities than $PANI_{10}$ samples since the ions are capable to diffuse faster into the PANI structure to access the surface of the substrate [12].

Fig. 8 shows the impedance modulus |z| vs. frequency plot for ACC, ACC/RGO_{15}, $ACC/PANI_{10}$ and $ACC/RGO_{15}PANI_{10}$. An impedance modulus, |z|, of around 40 Ω was measured for ACC at the lowest frequency of 0.01 Hz, directly related to the capacitive reactance. When ACC is coated with RGO and/or PANI, the value of the impedance modulus decreased significantly. $ACC/PANI_{10}$ and $ACC/RGO_{15}PANI_{10}$ coatings presented the best results because of the redox pseudocapacitance of PANI. The resistance of the samples measured at the highest frequencies (10000 Hz) decreases from 2.8 Ω for ACC to 0.9, 0.7 and 0.4 Ω for ACC/RGO_{15}, $ACC/PANI_{10}$ and $ACC/RGO_{15}PANI_{10}$, respectively. This result indicates, moreover, a good contact between the interface of ACC and the coated material.

To investigate the cyclic property of ACC, ACC/RGO_{15}, $ACC/PANI_{10}$ and $ACC/RGO_{15}PANI_{10}$, a 1000 cycles stability test was carried out at a current density of 1 A g^{-1}. In Fig. 9, ACC/RGO_{15} shows an increase of 38% with respect to ACC (124 F g^{-1}) after 1000 cycles. The curve of stability for ACC/RGO_{15} is almost a straight line with a gentle slope which indicates a good cycling performance. The specific capacitance of $ACC/PANI_{10}$ decreases sharply between the cycle numbers 400 and 600, to lose 20% of its initial capacitance (202 F g^{-1}). After that, the values of *Cs* became constant, and a 78% of its initial capacitance is retained. The stability curve for $ACC/RGO_{15}PANI_{10}$ shows a decay to cycle 500 (13%), maintaining 83% of its initial capacitance after 1000 cycles. These results indicate good cycling-stability of PANI on both ACC and ACC/RGO_{15} substrates without detachment of the PANI-coating. A 9% higher capacitance retention

and a smoother stability curve was observed for ACC/RGO_{15} which could be indicative of a certain synergetic effect caused by RGO.

In Table. 1, typical values of specific capacitance for graphene-PANI hybrid materials reported in literature are shown for comparison with those obtained in the present paper in which the electroactive material appears assembled into a flexible substrate.

3.4. Electrochemical study using a two-electrode symmetric cell configuration

In this section, the electrochemical behavior and performance of different samples were evaluated in a real capacitor constituted as a two-electrode cell. The CV-curves of the different samples are shown in Fig. 10a. A regular box-shaped characteristic for an ideal capacitor with good charge propagation was obtained for ACC and ACC/RGO_{15}. An increment in the CV-area is observed for ACC/RGO_{15} which means an about 27% increment with respect ACC according to charge-discharge curves of the Fig. 10b. These results are coherent with the charge-discharge curves obtained with the three-electrode cell in accordance with the equation (2): $Cs = 2C$ where C is the capacitance of the capacitor (two-electrode cell).

The CV-curves for ACC/$PANI_{10}$ and ACC/$RGO_{15}PANI_{10}$ show an area between -0.6 V an 0.6 V related to the redox-processes of PANI. An increment in CV-current is observed for the ACC/$RGO_{15}PANI_{10}$ sample which is indicative of the catalytic effect of RGO. Nevertheless, similar specific capacitances are obtained for ACC/$PANI_{10}$ and ACC/$RGO_{15}PANI_{10}$ according to charge-discharge curves. This could be caused by the reduction of the pseudo-capacitive contribution of PANI in the charge-discharge curves for the two electrode-cell configuration. To assess the deliverable performance for real-life applications, the energy and power densities were calculated [41, 42]. The specific energy density (W h Kg^{-1}) was calculated according to the equation $ED = C(\Delta V)^2/2$ where

C is the specific capacitance of the capacitor (two-electrode cell) and ΔV the operating potential range. The averaged specific power density (W Kg^{-1}) was calculated as $PD_{average} = ED/\Delta t$ where ED is the specific energy density and Δt the rate of discharge of the cell. ED-values of 33, 42, 50 and 49.4 W h Kg^{-1} are obtained for ACC, ACC/RGO_{15}, ACC/$PANI_{10}$ and ACC/$RGO_{15}PANI_{10}$ from the charge-discharge curves. These results are coherent since the energy power is directly proportional to the capacitance. The $PD_{average}$-values for ACC, ACC/RGO_{15}, ACC/$PANI_{10}$ and ACC/$RGO_{15}PANI_{10}$ were 990, 997, 986 and 1006 W Kg^{-1}, respectively. Higher values with regard to ACC are obtained for ACC/RGO_{15} and ACC/$RGO_{15}PANI_{10}$. According to the Ragone plot of energy density vs. power density for various energy-storing devices [43], the results of the present paper shows $PD_{average}$ values of a double-layer capacitor/supercapacitor [50-3000 W Kg^{-1}] with ED values of batteries [10-1000 W h Kg^{-1}].

4. Conclusions

In this work, the surface of a capacitive textile substrate is modified by using exclusively an electrodynamic method. ACC/RGO, ACC/PANI and ACC/RGOPANI samples, show a maximum improvement of 25%, 56% and 61% over the initial specific capacitance of ACC (about 129 F g^{-1}) and a good response in the 1000 cycles stability tests. It was proven that the maximum amount of electroactive material that it is possible to synthetize onto the textile surface to obtain an optimum response depends on the experimental conditions. The results obtained showed that RGO-coatings modified the PANI-polymerization process. The adsorption of aniline on RGO-coatings were detected. This adsorbed aniline was oxidized to obtain PANI. The morphology of the PANI-coating and the electrochemical properties of ACC and ACC/PANI are also influenced by RGO.

The methodology used in this paper opens a general route for the preparation of capacitive materials with dimensional versatility and high surface/mass and volume/mass ratios by electrodynamic methods.

5. Acknowledgements

The authors wish to acknowledge to Chemviron Carbon who kindly donated the ZORFLEX® activated carbon fabric. The authors wish to thank the Spanish Agencia Estatal de Investigación de Economía (AEI) and European Union (FEDER funds) for the financial support (contract MAT2016-77742-C2-1-P). Tim Vickers is gratefully acknowledged for help with the English revision.

6. Bibliography

[1] H. Marsh, E.A. Heinz, F.R. Reinoso, Introduction to Carbon Technologies, Publicaciones de la Universidad de Alicante, 1997.

[2] K. Kinoshita, Carbon: Electrochemical and physicochemical properties, Wiley, New York, 1988.

[3] T. Burchell, Carbon materials for advances technologies, Elsevier Science, 1999.

[4] J.A. Menéndez Díaz, I.M. Gullón, Types of carbon adsorbents and their production, in: T. Bandosz (Eds.), Activated carbon surfaces in environmental remediation, Elsevier, 2006, pp. 1−48.

[5] M. Zhong, Y. Song, Y. Li, Ch. Ma, X. Zhai, J. Shi, Q. Guo, L. Liu, Effect of reduced graphene oxide on the properties of an activated carbon cloth/polyaniline flexible electrode for supercapacitors application, J. Power Sources 217 (2012) 6−12.

[6] D.W. Wang, F. Li, J. Zhao, W. Ren, Z.G. Chen, J. Tan, Zh.S. Wu, I. Gentle, G.Q. Lu, H.M. Cheng, Fabrication of graphene/polyaniline composite paper via in situ anodic

electropolymerization for high-performance flexible electrode, ACS Nano 3 (2009) 1745−1752.

[7] Y.G. Wang, H.Q. Li, Y.Y. Xia, Ordered whisker like polyaniline grown on the surface of mesoporous carbon and its electrochemical capacitance performance, Adv. Mater. 18 (2006) 2619−2623.

[8] J. Yan, T. Wei, B. Shao, Z. Fan, W. Qian, M. Zhang, F.F. Wei, Preparation of a graphene nanosheet/polyaniline composite with high specific capacitance, Carbon 48 (2010) 487−493.

[9] K. Zhang, L.L. Zhang, X.S. Zhao, J. Wu, Graphene/polyaniline nanofiber composites as supercapacitor electrodes, Chem. Mater. 22 (2010) 1392−1401.

[10] K. Chen, L.F. Chen, Y. Chen, H. Bai, L. Li, Three-dimensional porous graphene based composite materials: electrochemical synthesis and application, J. Mater. Chem. 22 (2012) 20968−20976.

[11] Z. Gao, W. Yang, J. Wang, H. Yan, Y. Yao, J. Ma, B. Wang, M. Zhang, L. Liu, Electrochemical synthesis of layer-by-layer reduced graphene oxide sheets/polyaniline nanofibers composite and its electrochemical performance, Electrochim. Acta 91 (2013) 185−194.

[12] Q. Zhang, Y. Li, Y. Feng, W. Feng, Electropolymerization of graphene oxide/polyaniline composite for high-performance supercapacitor, Electrochim. Acta 90 (2013) 95−100.

[13] Y. Tang, N. Wu, Sh. Luo, Ch. Liu, K. Wang, L. Chen, One-step electrodeposition to layer-by-layer graphene-conducting-polymer hybrid films, Macromol. Rapid Comm. 33 (2012) 1780−1786.

[14] Y. Jin, M. Fang, M. Jia, In situ one-pot synthesis of graphene-polyaniline nanofiber composite for high-performance electrochemical capacitor, Appl. Surf. Sci. 308 (2014) 333−340.

[15] L. Zhang, D. Huang, N. Hu, Ch. Yang, M. Li, H. Wei, Zh. Yang, Y. Su, Y. Zhang, Three-dimensional structures of graphene/polyaniline hybrid films constructed by steamed water from high-performance supercapacitors, J. Power Sources 342 (2017) 1−8.

[16] N. Hu, L. Zhang, Ch. Yang, J. Zhao, Zh. Yang, H. Wei, H. Liao, Zh. Feng, A. Fisher, Y. Zhang, Zh.J. Xu, Three-dimensional skeleton networks of graphene wrapped polyaniline nanofibers: an excellent structure for high-performance flexible solid-state supercapacitors, Scientific Reports, 2016, 6:19777/DOI: 10.1038/srep19777.

[17] Ch. Yang, L. Zhang, N. Hu, Zh. Yang, Y. Su, Sh. Xu, M. Li, L. Yao, M. Hong,Y. Zhang, Rational design of sandwiched polyaniline nanotube/layered graphene/polyaniline nanotube papers for high-volumetric supercapacitors, Chem. Eng. J. 309 (2017) 89−97.

[18] Ch. Yang, L. Zhang, N. Hu, Zh. Yang, H. Wei, Zh.J. Xu, Y. Wang, Y. Zhang, Densely-packed graphene/conducting polymer nanoparticle papers for high-volumetric-performance flexible all-solid-state supercapacitors, Appl. Surf. Sci. 379 (2016) 206−212.

[19] S. Grover, Sh. Goel, V. Sahu, G. Singh, R.K. Sharma, Asymmetric supercapacitive characteristic of PANI embedded holey graphene nanoribbons, ACS Sustain. Chem. Eng. 3 (2015) 1460−1469.

[20] X.M. Feng, R.M. Li, Y.W. Ma, R.F. Chen, N.E. Shi, Q.L. Fan, W. Huang, OneStep electrochemical synthesis of graphene/polyaniline composite film and its applications, Adv. Funct. Mater. 21 (2011) 2989−2996.

[21] H. Wang, Q. Hao, X. Yang, L. Lu, X. Wang, Graphene oxide doped polyaniline for supercapacitors, Electrochem. Commun. 11 (2009) 1158–1161.

[22] Q. Hao, H. Wang, X. Yang, L. Lu, X. Wang, Morphology-controlled fabrication of sulfonated graphene/polyaniline nanocomposites by liquid/liquid interfacial polymerization and investigation of their electrochemical properties, Nano Res. 4 (2011) 323–333.

[23] H. Wang, Q. Hao, X. Yang, L. Lu, X. Wang, A nanostructured graphene/polyaniline hybrid material for supercapacitors, Nanoscale 10 (2010) 2164–2170.

[24] A.K. Geim, K.S. Novoselov, The rise of graphene, Nat. Mater. 6 (2007) 183−191.

[25] K.S. Novoselov, A.K. Geim, S.V. Morozov, D. Jiang, Y. Zhang, S.V. Dubonos, A.A. Grigorieva, A.A. Firsov, Electric field effect in atomically thin carbon films. Science 306 (2004) 666−669.

[26] K.S. Novoselov, D. Jiang, F. Scheding, T.J. Booth, V.V. Khotkevich, S.V. Morozov, A.K. Geim, Two-dimensional atomic crystals, Proc. Natl. Acad. Sci. USA 102 (2005) 10451−10453

[27] S.J. Choi, S.M. Park, Electrochemistry of conductive polymers. XXVI. Effects of electrolytes and growth methods on polyaniline morphology, J. Electrochem. Soc. 149 (2002) E26−E34.

[28] Z. Wang, X. Zhou, J. Zhang, F. Boey, H. Zhang, Direct electrochemical reduction of a single-layer graphene oxide and subsequent functionalization with glucose oxidase, J. Phys. Chem. C 113 (2009) 14071−1475.

[29] J. Molina, M.F. Esteves, J. Fernández, J. Bonastre, F. Cases, Polyaniline coated conducting fabrics. Chemical and electrochemical characterization, Eur. Polym. J. 47 (2011) 2003−2015.

[30] T. Ohsaka, Y. Ohnuki, N. Oyama, IR absorption spectroscopic identification of electroactive and electroinactive polyaniline films prepared by the electrochemical polymerization of aniline, J. Electroanal. Chem. 161 (1984) 399−405.

[31] N.S. Sariciftci, H. Kuzmany, H. Neugebauer, A. Neckel, Structural and electronic transitions in polyaniline: A Fourier transform infrared spectroscopy study, J. Chem. Phys. 92 (1990) 4530−4537.

[32] D.W. Hatchett, M. Josowicz, J. Janata, Comparison of chemically and electrochemically synthesized polyaniline films, J. Electrochem. Soc. 146 (1999) 4535–4538.

[33] J.L. Camalet, J. Lacroix, T.D. Nguyen, S. Aeiyach, M.C. Pham, J. Petitjean, P.C. Lacaze, Aniline electropolymerization on platinum and mild steel from neutral aqueous media, J. Electroanal. Chem. 485 (2000) 13−20.

[34] R. Hirase, T. Shikata, M. Shirai, Selective formation of polyaniline on wool by chemical polymerization, using potassium iodate, Synth. Met. 146 (2004) 73−77 [28] L. Wen, N.M. Kocherginsky, Doping-dependent ion selectivity of polyaniline membranes, Synth. Met. 106 (1999) 19−27.

[35] L. Wen, N.M. Kocherginsky, Doping-dependent ion selectivity of polyaniline membranes, Synth. Met. 106 (1999) 19−27.

[36] Merck FTIR Atlas, A collection of FTIR spectra, VCH, Merck,1988.

[37] G. Sócrates, Infrared Characteristic Group Frequencies, John Wiley & Sons, 1997.

[38] L. Jiang, Z. Cui, One-step synthesis of oriented polyaniline nanorods through electrochemical deposition, Polym. Bull. 56 (2006) 529−537.

[39] E.T. Kang, K.G. Neoh, K.L. Tan, Polyaniline: a polymer with many intrinsic redox states, Prog. Polym. Sci. 23 (1998) 277–324.

[40] N.P.S. Chauhan, R. Ametab, R. Ametac, S.C. Ametaa, Thermal and conducting behavior of emeraldine base (EB) form of polyaniline (PANI). Indian J. Chem. Techn. 18 (2011) 118–122.

[41] A. Laheäär, P. Przygocki, Q. Abbas, F. Béguin, Appropriate methods for evaluating the efficiency and capacitive behavior of different types of supercapacitors, Electrochem. Commun. 60 (2015) 21–25.

[42] B.K. Kim, S. Sy, A. Yu, J. Zhang, Electrochemical supercapacitors for energy storage and conversion, Handbook of Clean Energy Systems (2014) 1–25.

[43] Battery performance characteristics, Battery and energy technologies, http://www.mpoweruk.com/performance.htm

Figure Captions

Fig. 1. CV-curves for the synthesis of PANI on a WE recorded in 0.2 M aniline and 1 M H_2SO_4 solution at 5 mV s^{-1}.

Fig. 2. Second CV-cycle for the synthesis of RGO on a GCE (3 mm diameter) in 3 g L^{-1} GO and 0.1 M $LiClO_4 \cdot 3H_2O$ solution carried out between (a) -1.6 V to 0.6 V and (b) -1.8 V to 0.6 V at 50 mV s^{-1}.

Fig. 3. (a) and (b) CV-curves for the characterization of a sample of ACC and ACC/RGO_{15}. The scan rate was 20 mV s^{-1}. (c) and (d) Charge-discharge cycling curves for ACC and ACC/RGO_{15} at current densities of 1, 2, 3 and 4 A g^{-1}. (e) FESEM-image of ACC/RGO_{15} at 5 Kx.

Fig. 4. (a) and (b) first (i) and stabilized (s) CV-cycles recorded during the characterization of ACC/$PANI_{50}$ and ACC/$RGO_{15}PANI_{50}$ at 20 mV s^{-1}. (c) and (d) FESEM-images of ACC/$PANI_{50}$ at 500 x and 15 Kx, respectively. (e) and (f) FESEM-images of ACC/$RGO_{15}PANI_{50}$ at 500 x and 15 Kx, respectively.

Fig. 5. (a) and (b) first (i) and stabilized (s) CV-cycles recorded during the characterization of ACC/$PANI_{10}$ and ACC/$RGO_{15}PANI_{10}$ at 20 mV s^{-1}. (c) and (d) FESEM-images of ACC/$PANI_{10}$ at 15 Kx and 50 Kx, respectively. (e) and (f) FESEM-images of ACC/$RGO_{15}PANI_{10}$ at 15 Kx and 50 Kx, respectively.

Fig. 6. FTIR-plots of ACC and ACC/$PANI_{10}$. The spectra were recorded at 400 scans and with a resolution of 4 cm^{-1}.

Fig. 7. Charge-discharge curves at different current densities of 1, 2, 3 and 4 A g^{-1} for (a) ACC/$PANI_{50}$, (b) ACC/$RGO_{15}PANI_{50}$, (c) ACC/$PANI_{10}$ and (d) ACC/$RGO_{15}PANI_{10}$.

Fig. 8. Plot of the impedance modulus |z| vs. frequency for ACC, ACC/RGO_{15}, ACC/$PANI_{10}$ and ACC/$RGO_{15}PANI_{10}$.

Fig. 9. Long cycling stability test of ACC, ACC/RGO_{15}, ACC/$PANI_{10}$ and ACC/$RGO_{15}PANI_{10}$ at a current density of 1 A g^{-1}.

Fig. 10. (a) CV-curves for the characterization of ACC, ACC/RGO_{15}, ACC/$PANI_{10}$ and ACC/RGO_{15} $PANI_{10}$ at 20 mV s^{-1}. (b) Charge-discharge cycling curves for ACC, ACC/RGO_{15}, ACC/$PANI_{10}$ and ACC/RGO_{15} $PANI_{10}$ at 1 A g^{-1}. The experiments were carried out in the two-electrode cell.

Tables

Table. 1. Some examples of specific capacitance-values for graphene-PANI hybrid materials reported in the literature.

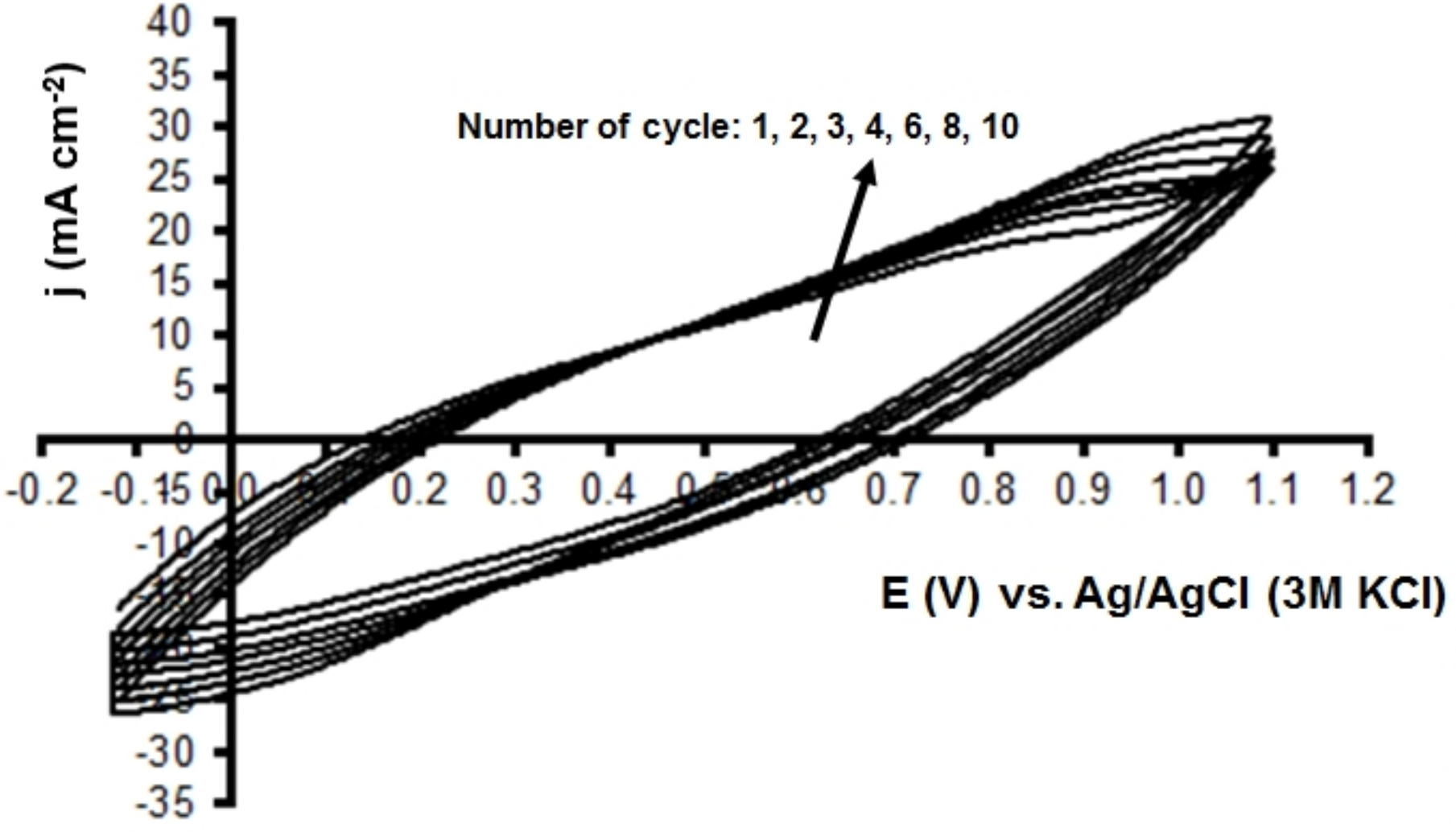
j (mA cm-2)
Number of cycle: 1, 2, 3, 4, 6, 8, 10
E (V) vs. Ag/AgCl (3M KCl)
40
35
30
25
20
15
10
5
0
-10
-30
-35
-0.2
-0.15
0.2
0.3
0.4
0.7
0.8
0.9
1.0
1.1
1.2

a

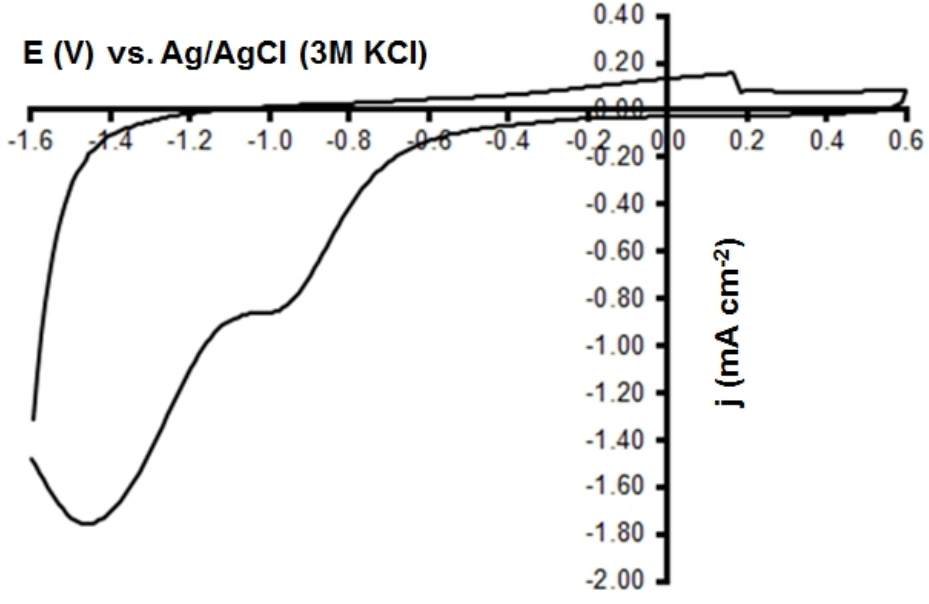
E (V) vs. Ag/AgCl (3M KCl)
0.40
0.20
0.00
-0.20
-0.40
-0.60
-0.80
-1.00
-1.20
-1.40
-1.60
-1.80
-2.00
-1.6
-1.4
-1.2
-1.0
-0.8
-0.6
-0.4
-0.2
0.0
0.2
0.4
0.6
j (mA cm-2)

b

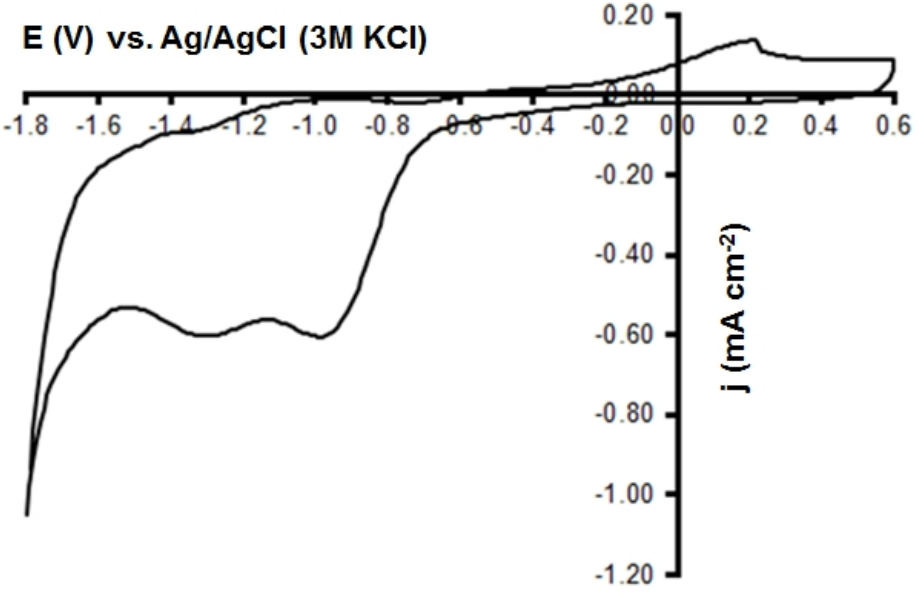
E (V) vs. Ag/AgCl (3M KCl)
0.20
0.00
-0.20
-0.40
-0.60
-0.80
-1.00
-1.20
-1.8
-1.6
-1.4
-1.2
-1.0
-0.8
-0.6
-0.4
-0.2
0.0
0.2
0.4
0.6
j (mA cm-2)

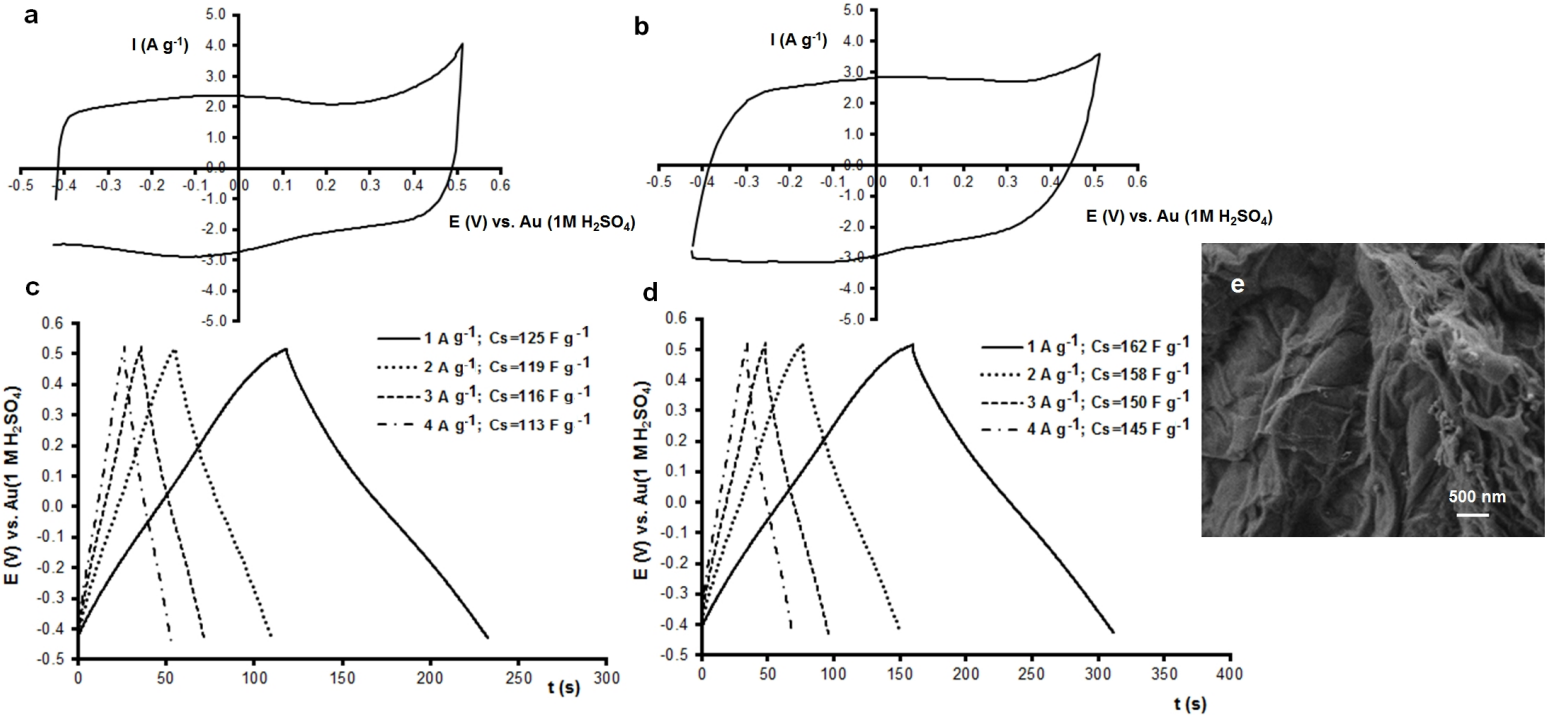
a
I (A g-1)
E (V) vs. Au (1M H2SO4)
b
I (A g-1)
E (V) vs. Au (1M H2SO4)
c
E (V) vs. Au(1 M H2SO4)
1 A g-1; Cs=125 F g-1
2 A g-1; Cs=119 F g-1
3 A g-1; Cs=116 F g-1
4 A g-1; Cs=113 F g-1
t (s)
d
E (V) vs. Au(1 M H2SO4)
1 A g-1; Cs=162 F g-1
2 A g-1; Cs=158 F g-1
3 A g-1; Cs=150 F g-1
4 A g-1; Cs=145 F g-1
t (s)
e
500 nm

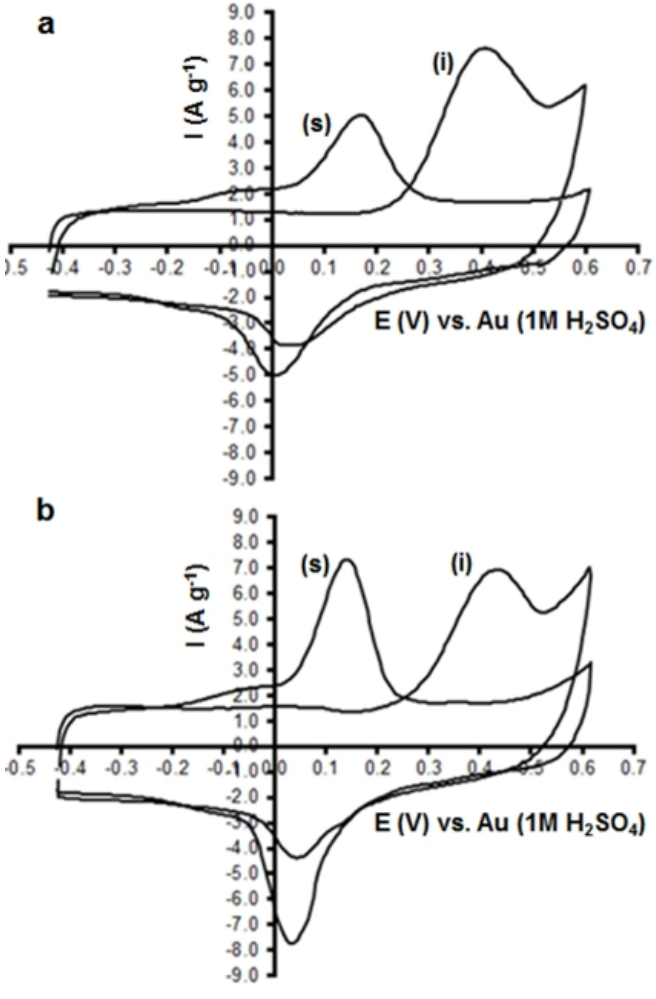
a
I (A g-1)
(s)
(i)
E (V) vs. Au (1M H2SO4)
b
I (A g-1)
(s)
(i)
E (V) vs. Au (1M H2SO4)

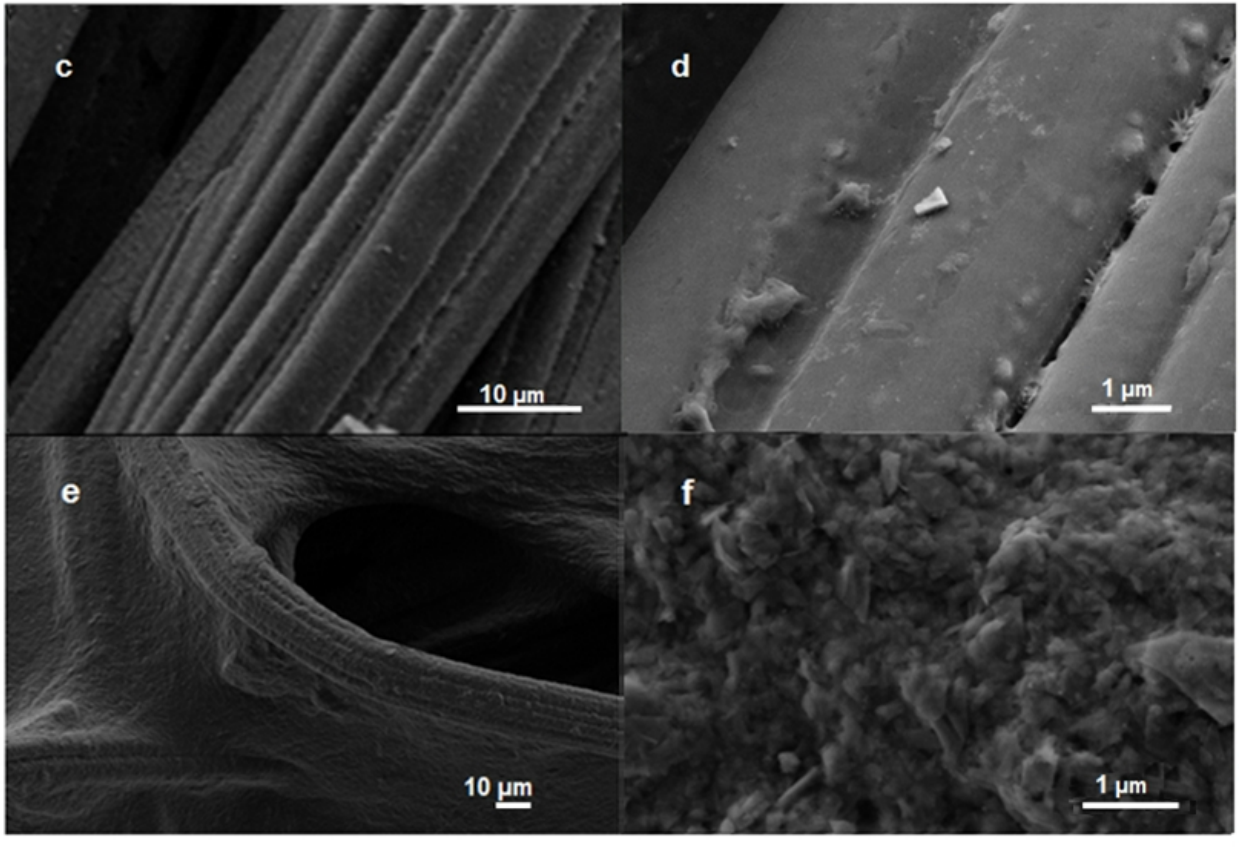
c
10 µm
d
1 µm
e
10 µm
f
1 µm

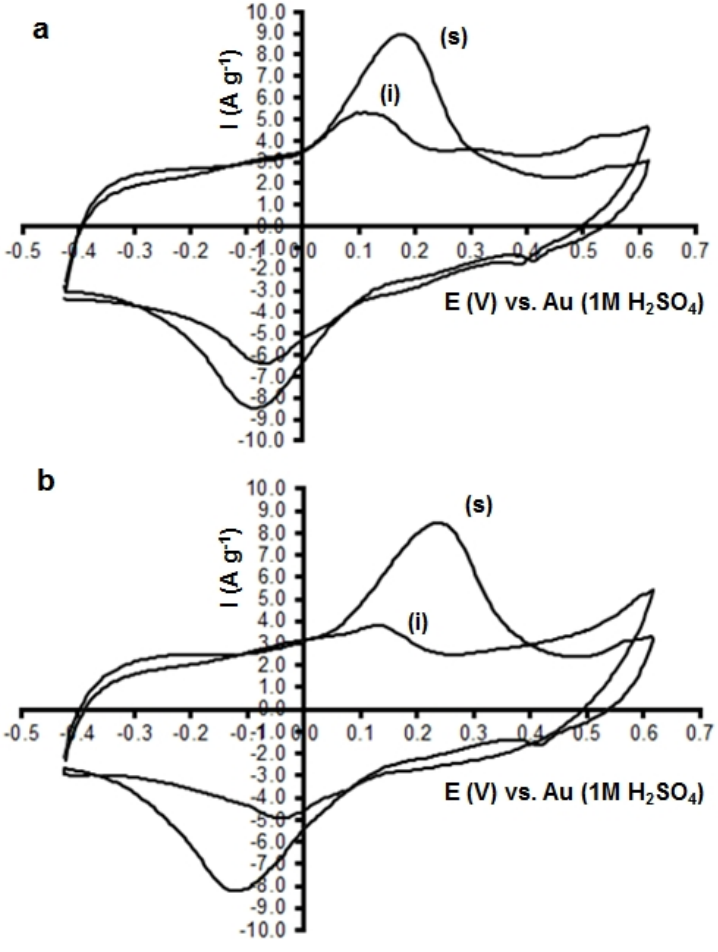
a
(s)
(i)
I (A g-1)
E (V) vs. Au (1M H2SO4)
b
(s)
(i)
I (A g-1)
E (V) vs. Au (1M H2SO4)

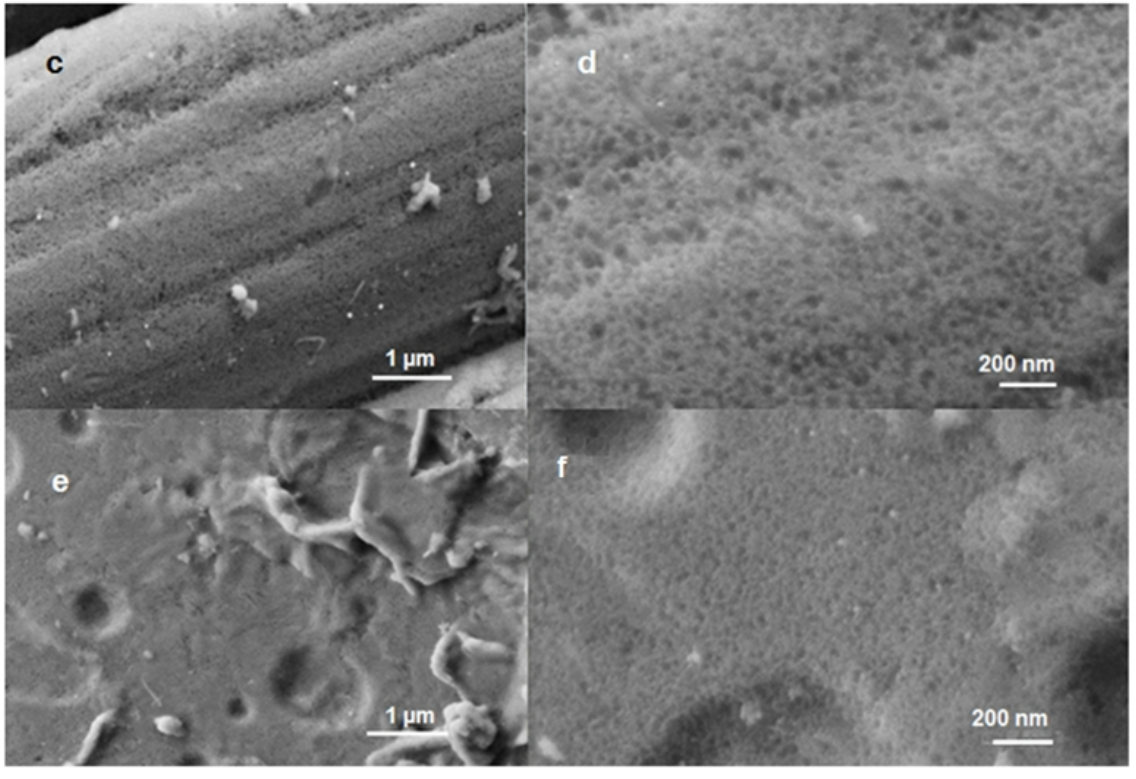
c
1 µm
d
200 nm
e
1 µm
f
200 nm

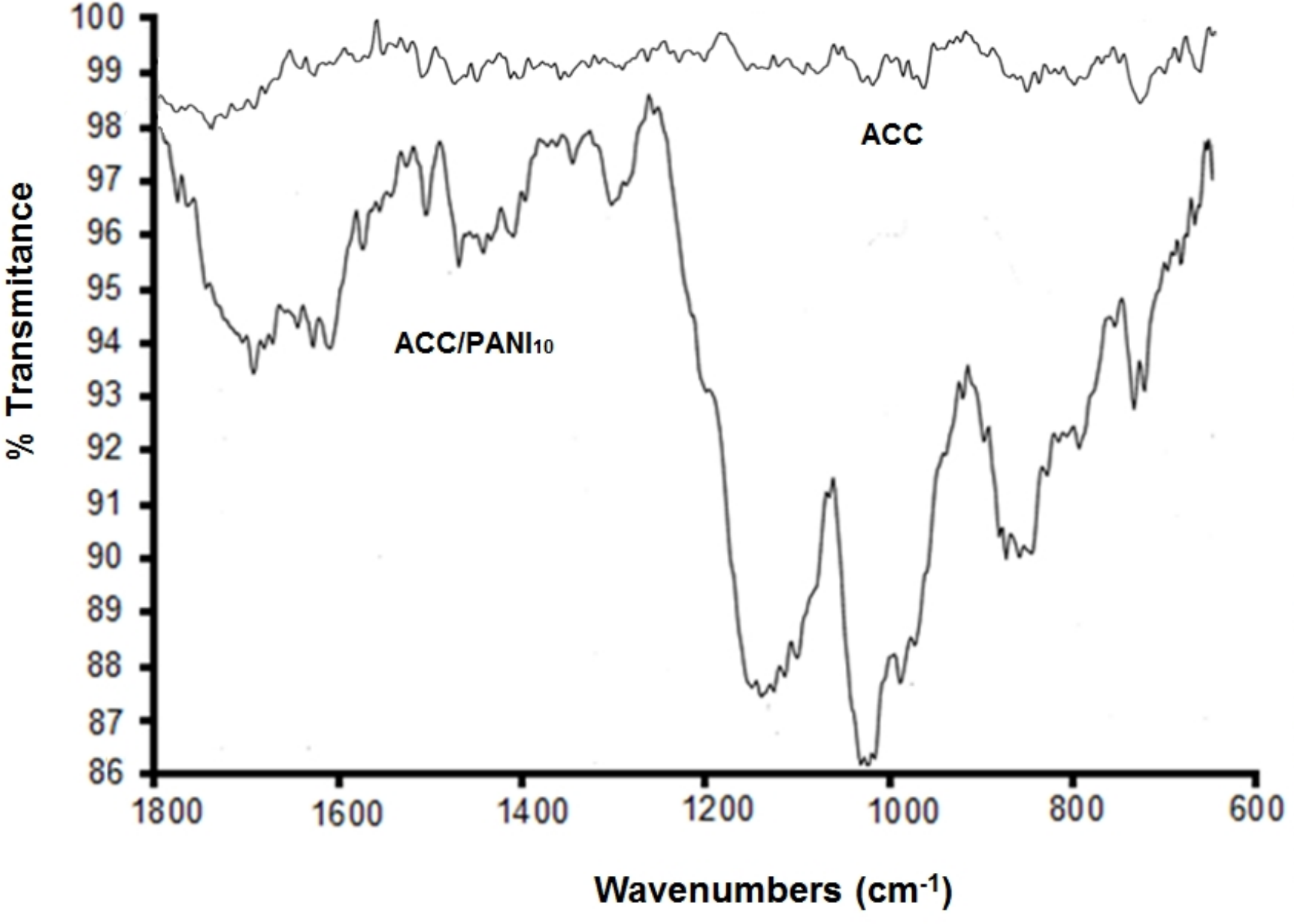
100
99
98
97
96
95
94
93
92
91
90
89
88
87
86
% Transmitance
ACC
ACC/PANI10
1800
1600
1400
1200
1000
800
600
Wavenumbers (cm-1)

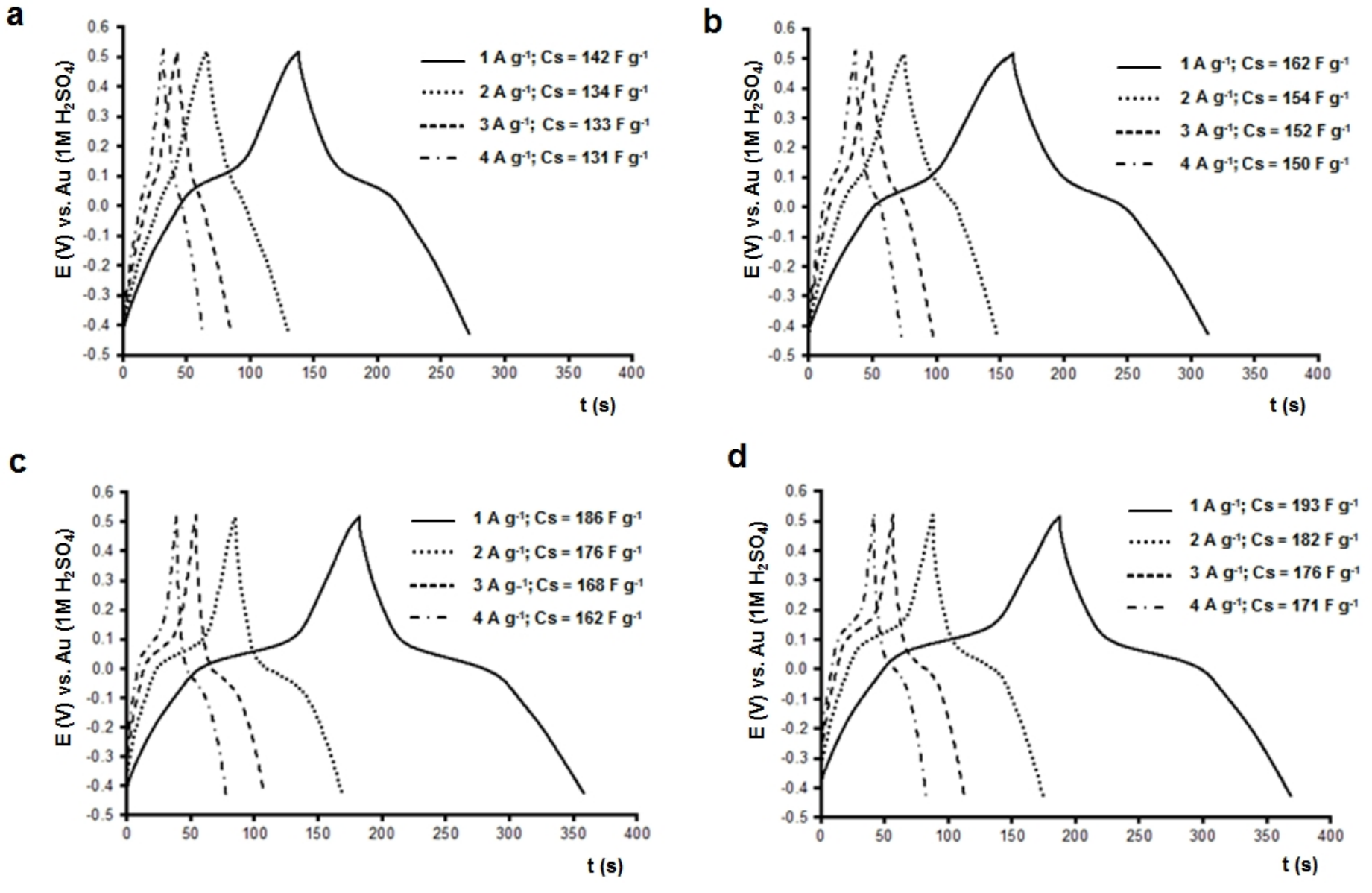
a
E (V) vs. Au (1M H_2SO_4)
t (s)
1 A g^{-1}; Cs = 142 F g^{-1}
2 A g^{-1}; Cs = 134 F g^{-1}
3 A g^{-1}; Cs = 133 F g^{-1}
4 A g^{-1}; Cs = 131 F g^{-1}
b
E (V) vs. Au (1M H_2SO_4)
t (s)
1 A g^{-1}; Cs = 162 F g^{-1}
2 A g^{-1}; Cs = 154 F g^{-1}
3 A g^{-1}; Cs = 152 F g^{-1}
4 A g^{-1}; Cs = 150 F g^{-1}
c
E (V) vs. Au (1M H_2SO_4)
t (s)
1 A g^{-1}; Cs = 186 F g^{-1}
2 A g^{-1}; Cs = 176 F g^{-1}
3 A g^{-1}; Cs = 168 F g^{-1}
4 A g^{-1}; Cs = 162 F g^{-1}
d
E (V) vs. Au (1M H_2SO_4)
t (s)
1 A g^{-1}; Cs = 193 F g^{-1}
2 A g^{-1}; Cs = 182 F g^{-1}
3 A g^{-1}; Cs = 176 F g^{-1}
4 A g^{-1}; Cs = 171 F g^{-1}

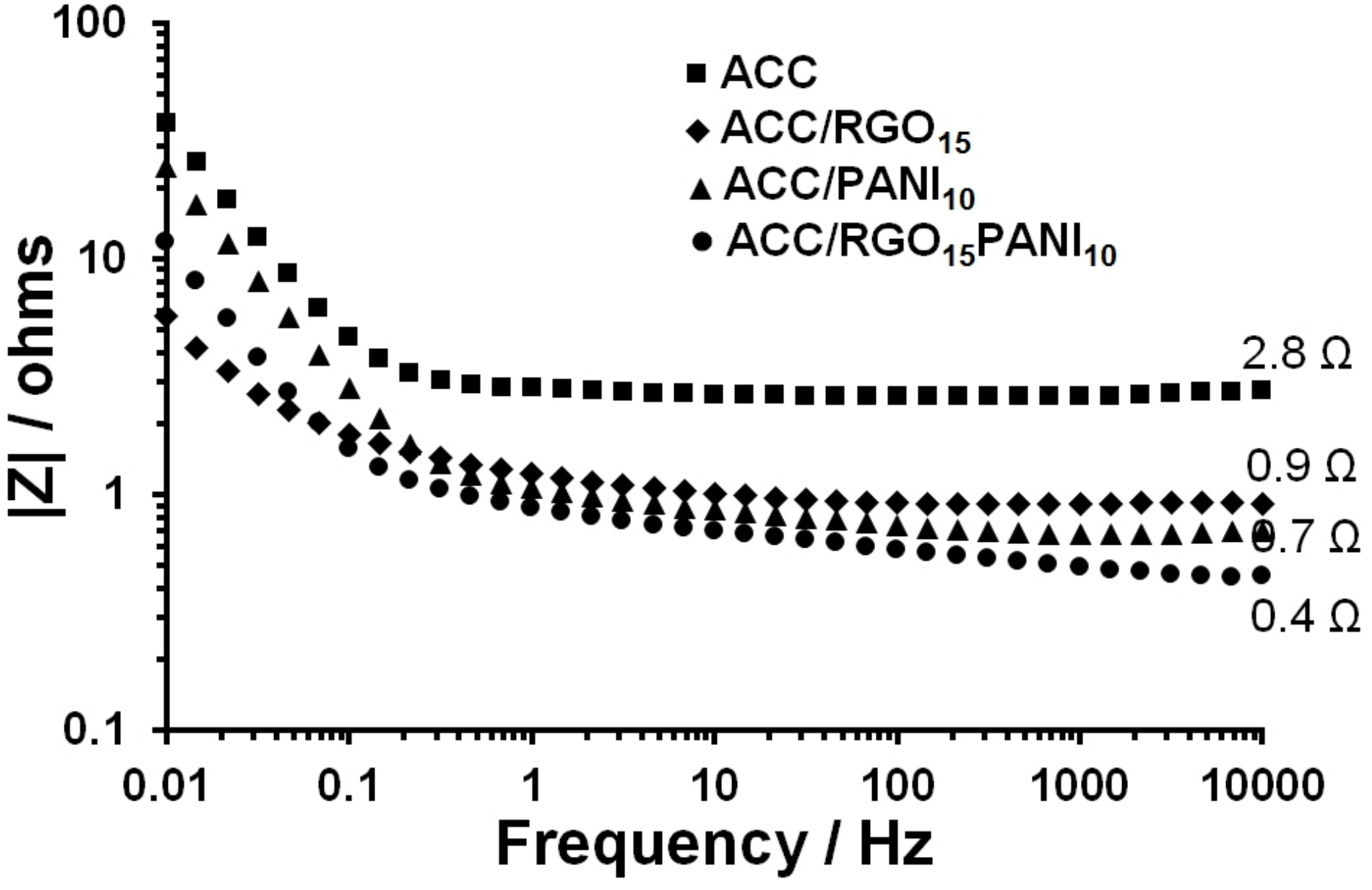
100
10
1
0.1
|Z| / ohms
0.01
0.1
1
10
100
1000
10000
Frequency / Hz
ACC
ACC/RGO15
ACC/PANI10
ACC/RGO15PANI10
2.8 Ω
0.9 Ω
0.7 Ω
0.4 Ω

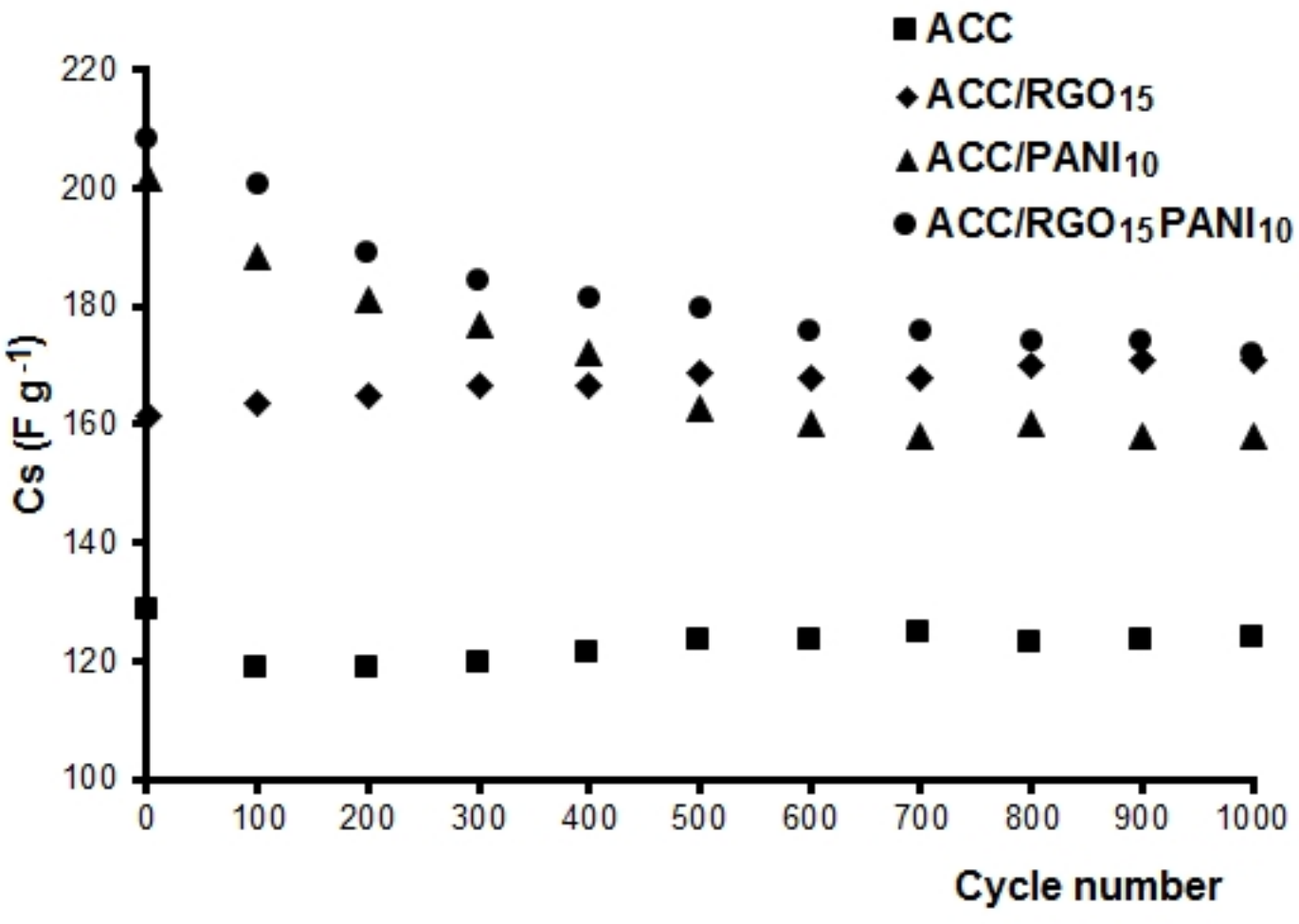
ACC
ACC/RGO15
ACC/PANI10
ACC/RGO15PANI10
Cs (F g-1)
220
200
180
160
140
120
100
0
100
200
300
400
500
600
700
800
900
1000
Cycle number

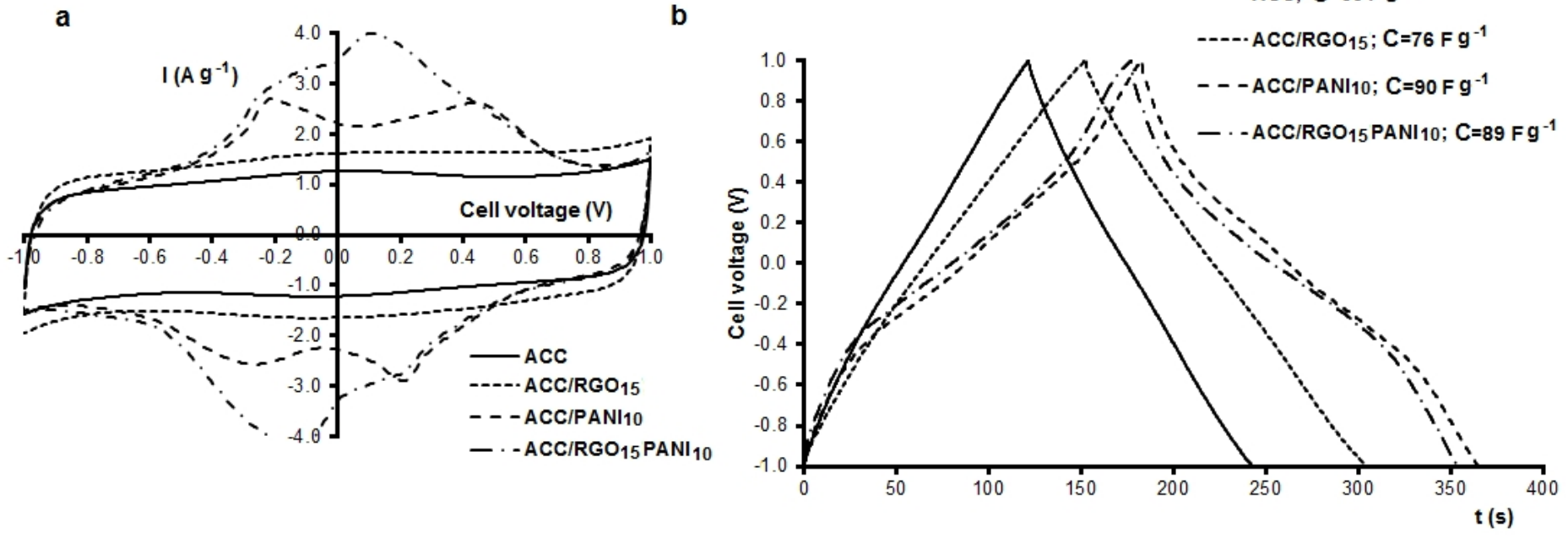
a
I (A g-1)
Cell voltage (V)
4.0
3.0
2.0
1.0
0.0
-1.0
-2.0
-3.0
-4.0
-1.0
-0.8
-0.6
-0.4
-0.2
0.0
0.2
0.4
0.6
0.8
1.0
ACC
ACC/RGO15
ACC/PANI10
ACC/RGO15PANI10
b
ACC; C=60 F g-1
ACC/RGO15; C=76 F g-1
ACC/PANI10; C=90 F g-1
ACC/RGO15PANI10; C=89 F g-1
Cell voltage (V)
t (s)
1.0
0.8
0.6
0.4
0.2
0.0
-0.2
-0.4
-0.6
-0.8
-1.0
0
50
100
150
200
250
300
350
400

Material composition	Specific capacitance (F g-1)	Method of synthesis	Ref.
PANI-fibers, GO, RGO, and PANIGOx, PANIRGOx composites	130 :PANI-f 219, 147, 148 :PANIGO$_{10,50,80}$ 179, 128, 200 :PANIRGO$_{10,50,80}$ at 1 A g-1	PANI-f: Chemical oxidation with $(NH_4)_2S_2O_8$; RGO: chemical reduction with N_2H_4.	9
Three-dimensional RGOPANI composite	102 :RGO 560 :RGOPANI at 1.4 A	PANI: Cyclic voltammetry in the range of 0 to 0.65 V RGO: Electrochemical reduction of GO at -1.15 V vs. saturated calomel electrode on a Cu foil electrode.	10
Graphene/PANI composite film	560 :RGOPANI at 0.1 A g-1	PANI: Cyclic voltammetry in the range of -1.3 and +1.0 V versus saturated calomel electrode on glassy carbon or indium tin oxide electrodes, from an aniline+GO suspension.	20
Activated carbon cloth (ACC), ACC/PANI and ACC/RGOPANI	200 :ACC 300 :ACC/PANI 325 :ACC/RGOPANI at 1 A g-1	PANI: Potentiostatic electrodeposition at 0.9 V vs. saturated calomel electrode; RGO: Chemical reduction with *p*-phenylene diamine.	5
Free standing and flexible RGOPANI composite paper	233 :RGOPANIpaper 147 :RGOpaper	PANI: Potentiostatic electrodeposition at 0.75 V vs. saturated calomel electrode; RGO: Hydrogen reduction of thermally expanded GO	6
Three-dimensional skeleton networks of graphene wrapped polyaniline nanofibers	211 :Assembled solid state at 1 A g-1	Hydrothermal reduction of GOPANI hydrogels by L-cysteine and then pressed on the carbon paper substrates under a pressure of ~1 MPa to form thin hydrogel films.	16
PANI nanotube-anchored graphene papers	363 :RGOPANI at 1 A g-1	PANI: Chemical oxidation with $K_2S_2O_8$; RGO: chemical reduction with N_2H_4.	17

Highlights

- A capacitive carbon cloth is modified exclusively by cyclic voltammetry.
- RGO/PANI modified cloth presents a 54% improvement in specific capacitance.
- Optimum amount of electroactive material is determined.
- RGO modifies morphology and electrochemical response of PANI.
- A route to obtain capacitive materials with dimensional versatility is opened.